ADVANCED MATERIALS

Anatase and Rutile TiO_2 Macrocellular Foams: Air–Liquid Foaming Sol–Gel Process Towards Controlling Cell Sizes, Morphologies, and Topologies**

By *Florent Carn*, *Annie Colin*, *Marie-France Achard*, *Hervé Deleuze*, *Clément Sanchez*, and *Rénal Backov**

Mesostructuration of inorganic materials is a rather well-established method today.[1] To achieve a higher degree of control over nanoporous or macroporous organized textures, mineralization can be confined to macroscopic interfaces, as demonstrated by the growing field of bio-inspired materials.[2] In this context, three main routes can be identified. The first approach makes use of macroscopic patterns via metastable thermodynamic systems (e.g., emulsions and reverse emulsions),[3,4] while the second is based on mesoscopic supramolecular templating effects where the induced inorganic texturation extends to longer length scales.[5] The third route relies upon a preformed microorganism[6] or pre-existing colloidal opal-like organic textures.[7] These strategies are leading to the new "chemistry of shapes" concept, and to "synthesis over all length scales".[8] In the context of the first route, we recently developed a new process that allows a high degree of control over the macroscopic cell sizes and morphologies of silica foam.[9] Beyond void-space texturation, an important task seems to be to associate specific properties with the inorganic scaffolds. In this context, there is a strong need for the development of innovative techniques for the well-controlled synthesis of high-surface-area foams and hierarchical shapes of titanium dioxide, with strong emphasis on environmental applications that include sorption media, filters, and photocatalysts for air or water purification.[10] Nevertheless, much more work is dedicated to silica than to titania. This observation certainly comes from the fact that the hydrolysis–condensation reactions involved in silica polymerization are much easier to control, even though recent work dealing with TiO_2 mesostructured thin films,[11] porous nanocrystalline foams,[7,12] hollow fibers,[13] nanotubes,[14] ribbons,[15] and microspheres[16] are emerging. Taking into account the environmental applications mentioned above, the first crucial parameter to be tuned is the nanostructure of the porous materials,[10,12] while the second important goal is to obtain monolith-type materials.

In the present paper, we describe the synthesis and characterization of TiO_2 macrocellular scaffolds by a rational air–liquid foaming sol–gel process. Here, both size and shape of the macroscopic cells, as well as thickness and texture of the macroscopic cell walls (i.e., the Plateau borders), can be tuned. Beyond control over the macroscale morphology at the microscopic length scale, these procedures allow the synthesis of amorphous TiO_2, monophasic crystalline anatase, biphasic anatase–rutile, or monophasic rutile TiO_2 compounds by increasing the thermal-treatment temperature. Using the synthesis described below, all the materials were obtained as monoliths (Fig. 1).

Figure 1. Titanium dioxide inorganic foam obtained as a monolith.

Using the non-static method developed in our previous study,[9] we were able to obtain complete control over the cell sizes and morphologies of silica macrocellular foams. By extending this process to TiO_2, we aim to tune the macroscopic cell morphologies by changing the starting air–liquid-foam liquid fractions (ρ), where ρ corresponds to the ratio of the volume of the liquid constituting the foam to the total foam volume. The relationship between ρ and the foam morphology can be expressed as[17]

$$\rho = 0.171(r/L_{PB})^2 + 0.256(r/L_{PB})^3 \approx a/L^2_{PB\,a}/L_{PB0.5}] \quad (1)$$

where r is the Plateau-border curvature, L_{PB} is the Plateau-border length, and a is the Plateau-border width. The foam-liquid fraction ρ can be tuned by varying the sol flux (Q) at the top of the foam. Using this drainage property, either polygonal (Figs. 2a,b) or spherical (Figs. 2c,d) TiO_2 macroscopic-cell morphologies can be obtained, starting from a sol composed of tetradecyltrimethylamonium bromide (TTAB) as the sur-

[*] Dr. R. Backov, F. Carn, Dr. M.-F. Achard
Centre de Recherche Paul Pascal, UPR 8641-CNRS
115 Avenue Albert Schweitzer, F-33600 Pessac (France)
E-mail: backov@crpp-bordeaux.cnrs.fr
Dr. A. Colin
Laboratoire Du Futur, UMR CNRS-Rhodia FRE2771
178 Avenue Albert Schweitzer, 33607 Pessac (France)
Dr. H. Deleuze
Laboratoire de Chimie Organique et Organométallique
UMR 5802-CNRS, Université Bordeaux 1
351 Cours de la Libération, F-33045 Talence Cedex (France)
Dr. C. Sanchez
Laboratoire de Chimie de la Matière Condensée, UMR-7574 CNRS
Université Pierre et Marie Curie
4 Place Jussieu, F-75252 Paris Cedex (France)

[**] The authors wish to thank Eric Lebreau (ICMCB-UPR 9048 CNRS) for the thermally assisted XRD data acquisition, Elizabeth Sellier (CREMEM-Université Bordeaux-1) for SEM picture acquisition, and Odile Babet (LCOO-Université Bordeaux-1) for the nitrogen physisorption data acquisition. This work is part of the 6th PCRDT REX European program (FAME-MIOH). Supporting Information is available online from Wiley InterScience or from the author.

  DOI: 10.1002/adma.200401080

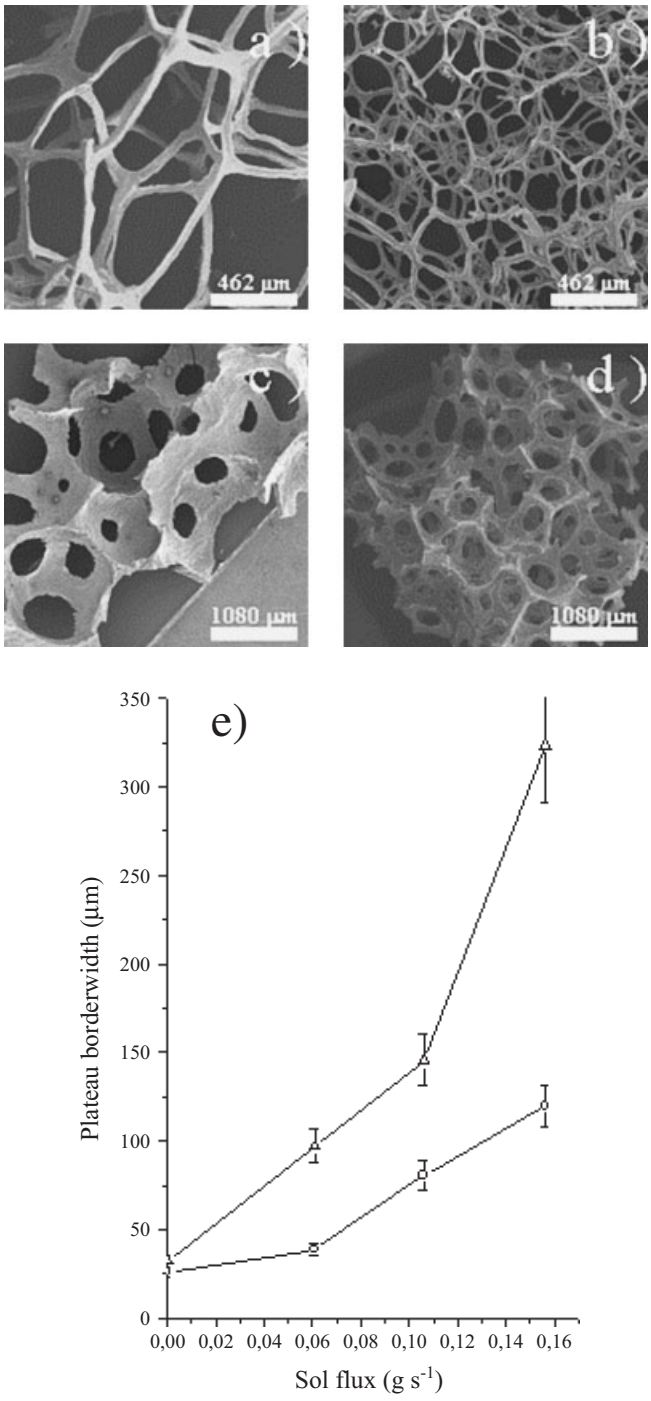

Figure 2. Evolution of the Plateau-border widths of the titanium dioxide scaffold with the sol flux (Q) corresponding to a bubbling-apparatus pore size of 130 µm: a) scanning electron microscopy (SEM) image of a hybrid TiO_2–tetradecyltrimethylamonium bromide (TTAB) foam (before calcination) obtained without wetting ($Q = 0$ g s^{-1}); b) SEM image of the same monolith after thermal treatment at 650 °C; c) SEM image of a hybrid TiO_2–TTAB foam (before calcination) obtained with $Q = 0.156$ g s^{-1}; d) SEM image of the same monolith after thermal treatment at 650 °C; and e) evolution of the Plateau-border widths as a function of Q (before (△) and after (○) thermal treatment).

factant and titanium ethoxide as the inorganic precursor (see Experimental). Beyond macroscopic-cell shapes, cell-wall thicknesses can be controlled to the extent that the foam-liquid fraction or sol flux can vary. Here, both the hybrid (non-calcined foam) and inorganic (calcined) TiO_2 Plateau-border thicknesses are dependant on the sol flux (Q) applied to the top of the starting air–liquid foams (Figs. 2a,c and Figs. 2b,d). Also, considering Figure 2, it is noticeable that the hybrid scaffolds endure strong shrinkage during the thermal treatment. This shrinkage (around 50 %) is higher than that associated with SiO_2 (around 30 %).[9] This high shrinkage is certainly induced by the sintering effect, enhanced for TiO_2 by crystallization, where the amorphous microstructure switches towards an ordered one. This thermal-transformation aspect and the mesoscale-organic-template removal will be discussed below. In order to tune the average macroscopic-cell sizes, we varied the porosity of the porous disk employed at the bottom of the column during the bubbling process (Fig. 3). We observed that the Plateau-border lengths, defined as the node-to-node distance, can vary from 100 µm to 580 µm for the hybrid foams, and then decrease to 60 µm and 200 µm, respectively, upon thermal treatment. As is the case for Plateau-border widths, the Plateau-border lengths are also subject to a strong shrinkage effect (Fig. 3e). In order to tune the mesoporosity of the inorganic scaffolds (as discussed below), we synthesized some TiO_2 macrocellular foams with sodium dodecylsulfate (SDS) as the surfactant. At the macroscopic length scale, we found that the Plateau-border textures are rather different from what we obtained with TTAB, and differ depending upon the aging time prior to exposing the sol to the foaming process. In Figures 4a,b, we observe that the Plateau-border texture is fibrous-like when the sol is aged for 20 h prior to performing the bubbling process. When the aging time was reduced to 30 min, the Plateau-border texture appears more homogeneous, with a ribbon-like morphology (Figs. 4c,d). This difference in topology might be due to a cooperative effect between the mesoscale SDS template, which for a 20 h aging time is certainly directing the inorganic growth at longer length scales, leading to the generation of high-aspect-ratio fibers. When this aging-time parameter was used with TTAB as the surfactant, we simply observed that the particle sizes increased with time, without any improvement in the particle aspect ratios (Fig. 1 in Supporting Information). This specific feature is very important, as TiO_2 can be used for photochemical therapy in the treatment of cancer cells.[10] Furthermore, bone osteoblast cells (cells involved in the generation of new bone) are very sensitive to the physical properties of their immediate surroundings, including surface composition, surface energy, roughness, and topography.[18] Therefore, apart from chemical composition, surface topography and roughness are key determinants in cell contact, growth, and osteointegration, as long as the open-cell diameters are larger than 100 µm.[19] As previously mentioned, apart from the shrinkage effect, thermal treatment enhanced

ADVANCED MATERIALS

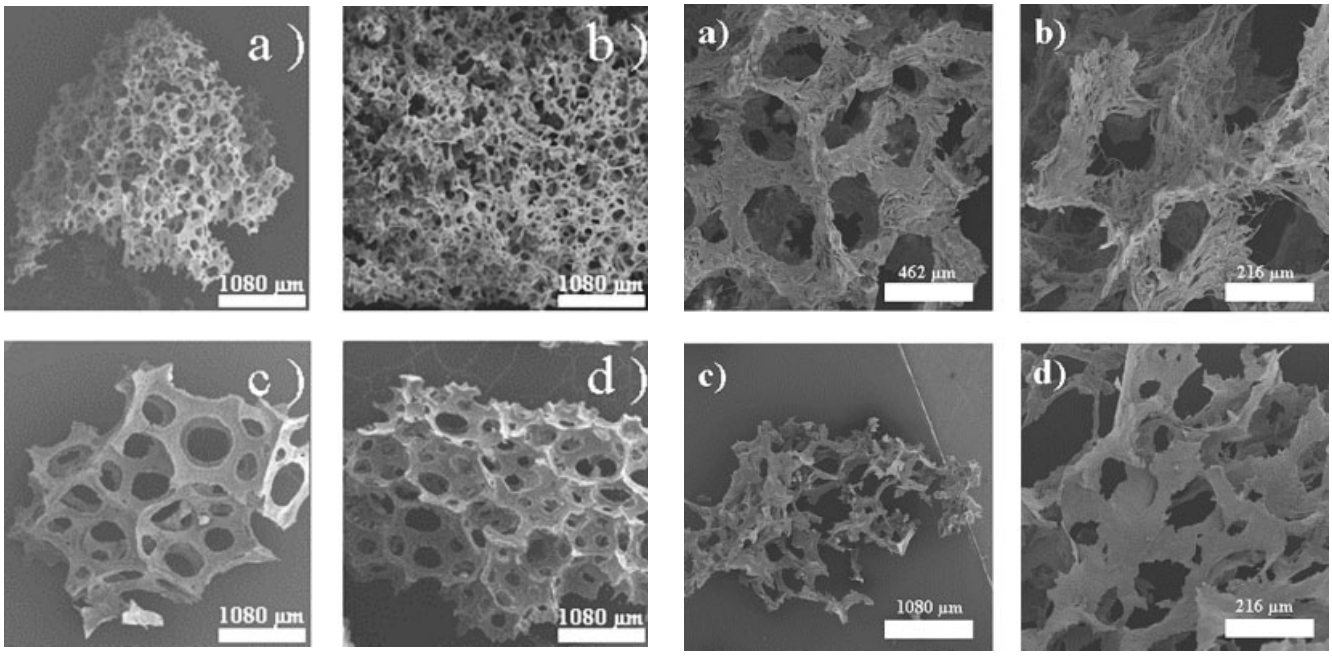

Figure 4. Evolution of the titanium dioxide Plateau-border topologies with the aging time imposed on the sol prior to performing the bubbling process for the foams obtained with SDS as surfactant and a bubbling-apparatus pore size of 130 µm: a) SEM image of a hybrid TiO_2–SDS foam (before calcination) with an aging time of 20 h; b) SEM image of the same monolith after thermal treatment at 500 °C; c) SEM image of a hybrid TiO_2–SDS foam (before calcination) with an aging time of 30 min; and d) SEM image of the same monolith after thermal treatment at 500 °C.

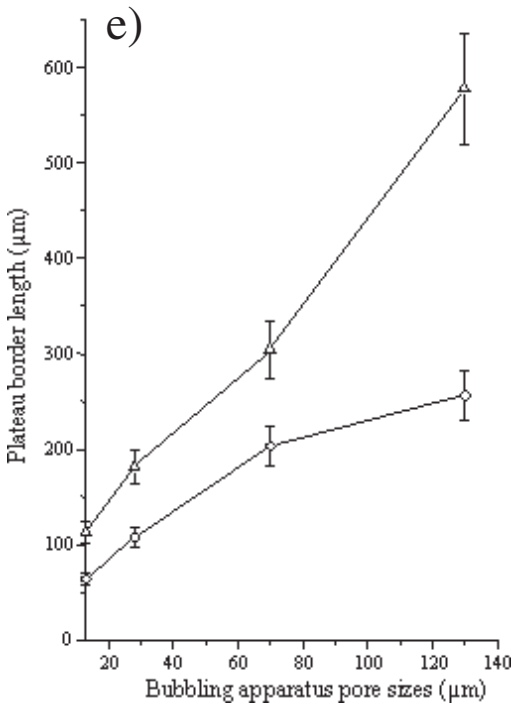

Figure 3. Evolution of Plateau-border lengths of the titanium dioxide scaffold with the type of porous disks used during the bubbling process for the same sol flux of $Q = 0.120$ g s^{-1}: a) SEM image of a hybrid TiO_2–TTAB foam (before calcination) obtained with a disk porosity of 10 µm; b) SEM image of the same monolith after thermal treatment at 650 °C; c) SEM image of a hybrid TiO_2–TTAB foam (before calcination) obtained with a disk porosity of 130 µm; d) SEM image of the same monolith after thermal treatment at 650 °C; and e) evolution of the Plateau-border lengths with the bubbling apparatus pore size (before (△) and after (○) thermal treatment).

the crystalline character of the TiO_2 microstructure. To appreciate this crystallization, X-ray diffraction (XRD) experiments have been performed on TTAB powders, TiO_2–TTAB hybrids, and TiO_2 inorganic scaffolds (Fig. 2, Supporting Information). The TTAB XRD pattern was indexed to the $P2_1/c$ space group,[20] and depicts lamellar organization from the small-angle (00l) Miller indices. The hybrid foam resembles pure TTAB powder, meaning that, as previously observed with SiO_2, TTAB microcrystallites certainly co-crystallize during the cold-lyophilization process. Also, no additional peaks are superimposed over the TTAB crystallographic peaks, indicating that the inorganic scaffold possesses an amorphous character. During thermal treatment of the hybrid materials at 300 °C, all the peaks associated with the organic matter disappear and new XRD patterns emerge. Those peaks can assigned to the Miller indices associated with the $I4_1/amd$ and $P4_2/mnm$ space groups, which characterize the TiO_2 anatase and rutile allotropic forms, respectively.[21,22] In order to assess the synthetic route presented here for its capability of obtaining an anatase TiO_2 foam as a monophasic system, we performed thermally-assisted XRD (Fig. 5). The 2θ window for this experiment was set as between 20–30° (2θ), as the [101]

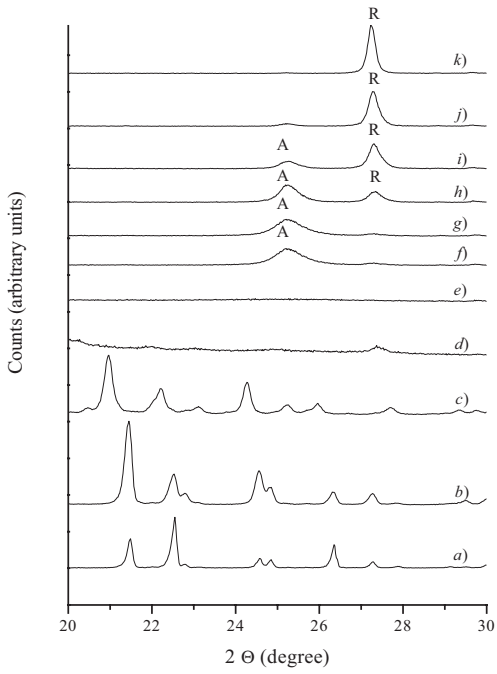

Figure 5. XRD patterns of titanium dioxide powders assessed with a thermal treatment: a) XRD pattern of TTAB powder; b) XRD pattern of a hybrid TiO_2–TTAB foam at room temperature; and at c) 100 °C, d) 200 °C, e) 300 °C, f) 400 °C, g) 500 °C, h) 600 °C, i) 700 °C, j) 800 °C, and k) 900 °C. The heating rate was 2 °C min^{-1}.

and [110] diffraction peaks of the anatase and rutile phases, respectively, are close enough to be followed simultaneously. In the first step, by heating the materials from ambient temperature to 100 °C, we observe a shift of the TTAB crystallographic peaks; furthermore, they become broader. This feature is certainly associated with organic-matter disorganization. Above 100 °C, and up to 300 °C, all the XRD TTAB peaks disappear, yielding a completely featureless XRD pattern at 300 °C. By increasing the temperature to 400 °C, the [101] anatase diffraction peak (A) emerges as a single peak until 600 °C is reached, where the native [110] rutile diffraction peak (R) can be observed. This experiment demonstrates that thermal treatment at 500 °C allows monophasic TiO_2 anatase macrocellular foams to be obtained. By increasing the temperature again, to above 500 °C, we obtain the biphasic anatase–rutile system, where the amount of the native rutile phase increases with temperature to finally reach the monophasic rutile state at 800 °C. This behavior is also observed when SDS is used as the surfactant, with some remnant SDS decomposition compounds present from 350–800 °C (Fig. 3, Supporting Information).

Apart from the sintering effect and the allotropic transformation, thermal treatment allows the evacuation of the organic part of the hybrid foams. Transmission electron microscopy (TEM) observations of the TiO_2 foam walls do not reveal the presence of mesoscale void-space texturation resulting from surfactant-template removal, as previously observed with silica.[9] The mesoporosity certainly arises from the void space induced by the random aggregation of nanoparticles within the foam walls, which varies both with the sol aging time and the surfactant ionic character (Fig. 1, Supporting Information). As a direct consequence, small-angle X-ray scattering experiments performed on these samples did not show any signature of mesoscale structuration, leading to poor mesoporosity. Also, the allotropic transformation associated with the thermal treatment enhances the crystalline character of the materials, thus avoiding microporosity. The nitrogen adsorption–desorption results are summarized in Table 1.

Table 1. Nitrogen physisorption data associated with the TiO_2 macrocellular-foam walls for the surfactants TTAB and SDS.

	Sol aging time [h]	Surface area [$m^2 g^{-1}$]	Surface area [a] [$m^2 g^{-1}$]
TTAB	0.5	58	67
	20	66	75
SDS	0.5	4	4
	20	12	10

[a] Calculated from the desorption curve.

In order to search for a stronger synergetic effect between the organization of lyotropic mesophases and the growing inorganic particles that might potentially optimize the mesostructuration, we varied the sol aging time (30 min and 20 h) prior to performing the air-bubbling process. The aging time imposed on the sol prior to performing the bubbling process does not demonstrate a strong effect upon the final mesoporosity, which remains low (Table 1) whatever the ionic character of the surfactant used. All other nitrogen adsorption–desorption curves and associated pore-size distribution plots of the as-synthesized materials are summarized in Figures 4–6 in the Supporting Information. In order to search for a higher mesoporosity, we performed the synthesis with Tergitol, a non-ionic surfactant, at different weight fractions. Unfortunately, this method does not result in self-supporting foams, i.e., the inorganic scaffolds collapse.

In conclusion, a TiO_2 sol–gel process associated with a non-static air–liquid bubbling process allows inorganic morphosynthesis, where, for the first time, polygonal- or spherical-macroscopic-cellular titania foams are obtained. Apart from the macroscopic-shape control, Plateau-border thicknesses and lengths can be tuned, almost on demand. Furthermore, this rational design is enhanced by the fact that the Plateau-border topologies can be varied from smooth textures to more fibrous-like or ribbon-like structures. The anatase- and rutile-derivative scaffolds might be useful in multiple applications, e.g., cell attachment and cancer-cell treatment, water treatment, and high-flux air purification. Future work will be dedicated towards testing these macrocellular foams for photocatalysis applications.

ADVANCED MATERIALS

Experimental

The foaming solutions were prepared by mixing a cationic surfactant (tetradecyltrimethylamonium bromide, TTAB) or an anionic surfactant (sodium dodecylsulfate, SDS), with water, titanium ethoxide, and HCl. Typically, titanium ethoxide was added to an aqueous solution of TTAB (35 wt.-%) or SDS (15 wt.-%) in order to reach a proportion of 10 wt.-%. Then, the pH of the solution was adjusted to pH = 1 by adding HCl (37 %). The mixture was subjected to strong stirring for 30 min to homogenize the solution and to evaporate ethanol produced by the hydrolysis of titanium alkoxide. A particulate sol could be obtained by aging for 20 h. Foam was obtained by bubbling nitrogen through a porous glass disk into perfluorohexane in a 2.5 cm-diameter, 60 cm-high Plexiglas column. Different porosity glass disks (100–160 μm, 40–100 μm, 16–40 μm, or 10–16 μm) could be used to introduce nitrogen into the foaming solution. The reaction took place inside the Plexiglas column. During the reaction, the foam was wetted from above with the foaming solution. Imposing a sol flux Q at the top of the foam allowed the imposition of a constant and homogeneous liquid fraction to the entire sample. Varying the sol flux Q at the top of the foam varied the liquid fraction, and thus tuned the morphology of the foam. Metastable foams were recovered at the top of the column with a spatula and stored in a beaker. Then, the foam was immediately treated with an aqueous ammonia solution (20 wt.-%) with a pipette in order to promote titanium dioxide condensation. The quantity of ammonia used during the process depended upon the foam-liquid fraction. Typically, we used 0.5 mL of ammonia solution for 100 mL of foam and a sol flux of 0.024 $g\,s^{-1}$, so the ratio was 2 mL/100 mL for a sol flux of 0.160 $g\,s^{-1}$. The final foams were then frozen overnight and lyophilized for 5 h. The resulting hybrid organic–inorganic monolith-type materials were then thermally treated at 500 °C in order to obtain the anatase structure of TiO_2, or at 900 °C to obtain the rutile structure. The heating rate was 2 °C min^{-1}, with a first Plateau at 200 °C for 2 h. The cooling process was uncontrolled and depended upon oven cooling. The final inorganic scaffolds were then analyzed.

Transmission electron microscopy (TEM) experiments were performed with a Jeol 2000 FX microscope (acceleration voltage of 200 kV). The samples were prepared as follows: TiO_2 scaffolds in a powder state were deposited on a copper grid coated with a Formvar/carbon membrane. Scanning electron microscopy (SEM) observations were performed with a Jeol JSM-840A SEM operating at 10 kV. The specimens were gold-coated or carbon-coated prior to examination. Mesoscale surface areas and pore characteristics were obtained with a Micromeritics ASAP 2010 instrument, employing the Brunauer–Emmett–Teller (BET) method. Prior to performing the nitrogen adsorption–desorption measurements, the macrocellular-foam monoliths were reduced to a powder state. Small-angle X-ray experiments were carried on with an 18 kW rotating-anode X-ray source (Rigaku-200) using a Ge (111) crystal as the monochromator. The scattered radiation was collected on a two-dimensional detector (Imaging Plate system from Mar Research, Hamburg). The sample–detector distance was 500 mm.

Received: July 6, 2004
Final version: October 11, 2004

[1] a) C. T. Kresge, M. E. Leonowicz, W. J. Roth, J. C. Vartuli, J. S. Beck, *Nature* **1992**, *359*, 710. b) J. S. Beck, J. C. Vartuli, W. J. Roth, M. E. Leonowicz, C. T. Kresge, K. D. Schmitt, C. T.-W. Chu, D. H. Olson, E. W. Sheppard, S. B. McCullen, J. B. Higgins, J. L. Schlenker, *J. Am. Chem. Soc*. **1992**, *114*, 10 834.

[2] a) S. Mann, *Nature* **1988**, *332*, 119. b) D. D. Archibald, S. Mann, *Nature* **1993**, *364*, 430. c) P. Feng, X. Bu, G. D. Stucky, D. J. Pine, *J. Am. Chem. Soc*. **2000**, *5*, 994. d) H. Yang, A. Kuperman, N. Coombs, S. Mamiche-Afara, G. A. Ozin, *Nature* **1996**, *379*, 703.

[3] a) A. Imhof, D. J. Pine, *Nature* **1997**, *389*, 948. b) S. Schacht, Q. Huo, I. G. Voigt-Martin, G. D. Stucky, F. Schüth, *Science* **1996**, *273*, 768. c) F. Carn, A. Colin, M.-F. Achard, E. Sellier, M. Birot, H. Deleuze, R. Backov, *J. Mater. Chem*. **2004**, *14*, 1370.

[4] G. Fornasieri, S. Badaire, R. Backov, O. Mondain-Monval, C. Zakri, P. Poulin, *Adv. Mater*. **2004**, *16*, 1094.

[5] J. H. Jung, Y. Yoshiyuki, S. Shinkai, *Angew. Chem. Int. Ed*. **2000**, *39*, 1862.

[6] S. R. Hall, H. Bolger, S. Mann, *Chem. Commun*. **2003**, 2784.

[7] D. Wang, R. A. Caruso, F. Caruso, *Chem. Mater*. **2001**, *13*, 364.

[8] a) S. M. Yang, I. Sokolov, N. Coombs, C. T. Kresge, G. A. Ozin, *Adv. Mater*. **1999**, *11*, 1427. b) G. A. Ozin, *Chem. Commun*. **2000**, 419. c) S. Mann, G. A. Ozin, *Nature* **1996**, *382*, 313.

[9] F. Carn, A. Colin, M.-F. Achard, H. Deleuze, R. Backov, *Adv. Mater*. **2004**, *16*, 140.

[10] a) A. Fujishima, K. Hashimoto, T. Watanabe, *TiO_2 Photocatalysis: Fundamentals and Applications*, BKC, Tokyo, Japan **1999**. b) M. Alfonso, D. Bahnemann, A. E. Cassano, R. Dilert, R. Goslich, *Catal. Today* **2000**, *58*, 199.

[11] E. L. Crepaldi, G. J. A. A. Soler-Illia, D. Grosso, F. Cagnol, F. Ribot, C. Sanchez, *J. Am. Chem. Soc*. **2003**, *125*, 9770.

[12] I. M. Ioannis, P. Falars, *Nano Lett*. **2003**, *3*, 249.

[13] S. Kobayashi, K. Hanabusa, N. Hamasaki, M. Kimura, H. Shirai, S. Shinkai, *Chem. Mater*. **2000**, *12*, 1523.

[14] Z. R. Tian, J. A. Voigt, J. Liu, B. McKenzie, H. Xu, *J. Am. Chem. Soc*. **2003**, *125*, 12 384.

[15] J. H. Jung, H. Kobayashi, K. J. C. van Bommel, S. Shinkai, T. Shimizu, *Chem. Mater*. **2002**, 14, 1445.

[16] T. Nakashima, N. Kimizuka, *J. Am. Chem. Soc*. **2003**, *125*, 6386.

[17] R. Phelan, D. Weare, E. A. J. F. Peters, G. Verbist, *J. Phys.: Condens. Matter* **1996**, *8*, 475.

[18] Z. Schwartz, C. H. Lohmann, J. Oefinger, L. F. Bonewald, D. D. Dean, B. D. Boyan, *Adv. Dent. Res*. **1999**, *13*, 510.

[19] A. Rezania, K. Healy, *Biotechnol. Prog*. **1999**, *15*, 755.

[20] A. Norbert, B. Brun, C. Dara, *Bull. Soc. Fr. Mineral. Cristallogr*. **1975**, *98*, 111.

[21] *Natl. Bur. Stand. (U.S.) Monogr*. **1969**, *25*, 82.

[22] *Natl. Bur. Stand. (U.S.) Monogr*. **1969**, *25*, 83.

A Hybrid Planar–Mixed Molecular Heterojunction Photovoltaic Cell**

By *Jiangeng Xue*, *Barry P. Rand*, *Soichi Uchida*, and *Stephen R. Forrest**

The interest in photovoltaic (PV) devices has long been motivated by the need to replace depleting, polluting fossil fuels with the clean and renewable alternative of solar energy.[1] Organic materials, both small molecules and conjugated polymers, have the potential to offer low-cost solar energy conversion due to their light weight, low cost, and compatibil-

[*] Prof. S. R. Forrest, Dr. J. Xue, B. P. Rand, Dr. S. Uchida[+]
Department of Electrical Engineering and Princeton Institute for the Science and Technology of Materials (PRISM)
Princeton University
Princeton, NJ 08544 (USA)
E-mail: forrest@princeton.edu

[+] Present address: Central Technical Research Laboratory, Nippon Oil Corporation, 8 Chidori-cho, Naka-ku, Yokohama, 230-0815, Japan.

[**] We gratefully acknowledge the National Renewable Energy Laboratory, the Air Force Office of Scientific Research, and Global Photonic Energy Corporation for partial support of this work.

  DOI: 10.1002/adma.200400617